HUMAN GENE THERAPY 23:891–902 (August 2012)

DOI: 10.1089/hum.2012.052

Safety Study of Adeno-Associated Virus Serotype 2-Mediated Human Acid Sphingomyelinase Expression in the Nonhuman Primate Brain

Ernesto A. Salegio,[1] Lluis Samaranch,[1] Russell W. Jenkins,[2] Christopher J. Clarke,[2,3] Clementine Lamarre,[1] Janine Beyer,[1] Adrian P. Kells,[1] John Bringas,[1] Waldy San Sebastian,[1] R. Mark Richardson,[1] Kate H. Rosenbluth,[1] Yusuf A. Hannun,[2,3] Krystof S. Bankiewicz,[1] and John Forsayeth[1]

Abstract

Niemann-Pick disease is a lysosomal storage disorder resulting from inherited deficiency in acid sphingomyelinase (ASM). Use of adeno-associated virus serotype 2 (AAV2) to deliver human acid sphingomyelinase (hASM) is currently being explored as a means to treat the devastating neurological features of NPD, which are refractory to traditional enzyme replacement therapy. In this study, we evaluated the long-term efficacy and safety of AAV2-hASM after direct infusion into the CNS of nonhuman primates. First, we confirmed the efficacy of AAV2-hASM in naive rats, which exhibited increased ASM expression and enzyme activity after infusion, without evidence of local or systemic toxicity. Next, the model was adapted to naive nonhuman primates (NHPs) with various doses of AAV2-hASM or saline delivered into the brainstem and both thalami. Strikingly, NHPs that received a high dose of AAV2-hASM displayed significant motor deficits that were not seen in low-dose animals in both the short-term (3-month) and long-term (9-month) treatment groups. In treated NHPs, ASM expression and activity were elevated with associated alterations in the sphingolipidomic profile in brain regions transduced with AAV2-hASM. Initial histological analysis indicated marked inflammatory reactions, and immunohistochemical analysis confirmed a robust inflammatory response. Importantly, pronounced up-regulation of the chemokine CCL5, a target of ASM-mediated inflammatory signaling, was detected that correlated with the inflammatory response, providing a possible mechanism for hASM-associated toxicity. This study defines dose-dependent and dose-independent toxicities of AAV2-hASM in the naive primate brain, and reveals potential challenges in the design of a clinical trial.

Introduction

Niemann-Pick disease (NPD) is a lysosomal storage disorder (LSD) resulting from a deficiency in acid sphingomyelinase (ASM) activity that is characterized by the accumulation of metabolic intermediates that interfere with normal cellular function, namely sphingomyelin (SM) and cholesterol. NPD types A and B are both caused by mutations in ASM that result in visceral complications such as hepatosplenomegaly. However, of the two, only type A (NPDA) is associated with a significant neurological deficit, and this difference is most probably due to the different levels of residual enzyme activity in various tissues. For instance, patients with NPD type B exhibit residual ASM activity ranging from 5 to 10%, compared with 1 to 2% observed in NPDA (Graber *et al.*, 1994). The fact that such a modest elevation in ASM activity appears to prevent the development of neurological disease in NPD suggests that genetic repair therapy is, therefore, an important avenue to explore because replacement of the defective gene in most cases should result in considerable therapeutic benefit.

Several strategies for enzyme replacement in LSD have been explored, with the goal of restoring enzymatic activity to a clinically effective level. Recombinant ASM purified from the culture medium of Chinese hamster ovary (CHO) cells (He *et al.*, 1999) is rapidly taken up from the circulation

[1]Department of Neurosurgery, University of California San Francisco, San Francisco, CA 94103.
[2]Department of Biochemistry and Molecular Biology, Medical University of South Carolina, Charleston, SC 29425.
[3]Present address: Department of Medicine and the Stony Brook University Cancer Center, Stony Brook University, Health Science Center, Stony Brook, NY 11794.

of ASM knockout mice primarily into liver and spleen, where it is directed to acidified organelles and can degrade SM (Miranda *et al.*, 2000). This finding strongly suggests that enzyme replacement therapy by intravenous infusion of recombinant ASM is a feasible strategy for the treatment of the peripheral symptoms of Niemann-Pick disease as seen in both types A and B. However, recombinant ASM does not cross the blood–brain barrier and, therefore, this therapy does not appear to improve ASM levels in the brain or reduce SM (Miranda *et al.*, 2000). It is essential, therefore, that alternatives to enzyme replacement therapies be developed to deal with the profound neurological deficits encountered in NPDA.

Direct gene therapy has considerable potential for the CNS-related effects of LSD. Gene therapy vectors have undergone a decade of development and discovery that has resulted in great advances in both efficacy and safety. Various vectors such as adenovirus (Peltola *et al.*, 1998; Amalfitano *et al.*, 1999; Ziegler *et al.*, 1999), lentivirus (Bosch *et al.*, 2000; Kim *et al.*, 2004), and adeno-associated virus have been used in a number of models of LSD (Barranger and Novelli, 2001; Hsich *et al.*, 2002; Watson and Wolfe, 2003). The ASM knockout mice develop neurological deficits due to massive loss of Purkinje cells in the cerebellum (Otterbach and Stoffel, 1995), thus mimicking the phenotype of the human disease (Kitagawa, 1987; Otterbach and Stoffel, 1995; Zhou *et al.*, 1995). The efficacy studies most relevant to the present work, however, are those in which ASM knockout mice received AAV-hASM (Dodge *et al.*, 2005; Passini *et al.*, 2005, 2007). In particular, Passini and colleagues (2005) showed that treatment with AAV2-hASM (1) corrected the distended lysosome pathology (2), restored normal cholesterol levels in brain (secondary substrate), and that AAV particles (3) can undergo axonal transport to distal areas of brains, despite the fact that projection neurons are sick at the time of injection (i.e., disease-compromised neurons support transport of AAV).

A major challenge in gene therapy has been the task of achieving global distribution of therapeutic agents within the CNS (Cearley and Wolfe, 2007). Thus, the choice of vector serotype and the target site are important considerations. In a study conducted in nonhuman primates (NHPs), we demonstrated that infusions of AAV2-hASM vector could be delivered accurately into motor-sensitive regions such as the brainstem and thalamus, without acute adverse side effects from the procedure (Salegio *et al.*, 2010). Therefore, to determine any long-term effects associated with the delivery of this vector into an ASM-rich environment such as the naive CNS of rats and NHP, we first determined the bioactivity of the ASM transgene by infusing it into the rat thalamus at the highest feasible dose and found robust ASM expression and enzyme activity. We then conducted short-term (3-month) and long-term (9-month) safety studies in NHPs with this delivery approach at two different doses of vector. Western blotting and an enzymatic assay revealed significant augmentation of human ASM (hASM) in the thalamus of both dose groups. Concomitantly, ASM-treated NHPs lost weight and developed neurological deficits not observed in phosphate-buffered saline (PBS)-infused controls. Histopathological examination of CNS tissue revealed robust infiltration of inflammatory cells in these animals. Recruitment and activation of immune cells were found in regions of hASM neuronal transduction, where hASM-positive neurons coexpressed a leukocyte chemokine (CCL5). CCL5 has been identified in a screen for novel effectors of ASM (Jenkins *et al.*, 2011), and was determined to be both necessary and sufficient for induction of CCL5 in both gain-of-function and loss-of-function models. Significantly, CCL5 was the only cytokine/chemokine (from a panel of more than 30) that was influenced by ASM. Last, sphingolipidomic analysis indicated a reduction in SM, and a surprising decrease in the levels of ceramide (the immediate product of SM metabolism), with associated increases in the levels of sphingosine and sphingosine 1-phosphate. We conclude that, in naive animals already expressing normal endogenous ASM, the exogenous administration and transduction of neurons to overexpress this enzyme induces neuropathological side effects.

Materials and Methods

Animals

Twenty Sprague-Dawley rats ($\sim$250–350 g) were allocated into two groups. The treatment group ($n=15$) received unilateral thalamic infusions of 15 μl of AAV2-hASM and the control group ($n=5$) received unilateral thalamic infusions of PBS. The period between vector infusion and necropsy was 3 months in all cases. To translate the results from our rodent experiments, we included eight NHPs (*Cynomolgus*) in this study. These were randomized to treatment groups comprising 3-month survival ($n=4$) and 9-month survival ($n=2$) from the date of vector administration and a 3-month ($n=2$) cohort infused with PBS to serve as controls. All animals received bilateral infusions of 125 μl (vector or PBS) per thalamus and 200 μl unilaterally in the brainstem. All animal handling and procedures were carried out in accordance with the University of California San Francisco (San Francisco, CA) Institutional Animal Care and Use Committee.

Adeno-associated viral vector

AAV serotype 2 vector carrying cDNA sequence encoding human acidic sphingomyelinase (hASM) downstream from a cytomegalovirus (CMV) promoter was packaged at the clinical Vector Core facility at Children's Hospital of Philadelphia (Philadelphia, PA) (Matsushita *et al.*, 1998; Ayuso *et al.*, 2010). Undiluted vector was used for the rats (thalamus only) and for the high-dose NHPs (4.3×10^{12} vector genomes/ml) and this was diluted 10-fold with vehicle (PBS–0.001% Pluronic [v/v]; Invitrogen, Carlsbad, CA) for lower doses.

Surgery and AAV2-hASM infusion

Rats were anesthetized with isoflurane (Baxter, Deerfield, IL) and placed in a stereotactic frame (David Kopf Instruments, Tujunga, CA). A 1-cm longitudinal incision was made in the skin overlaying the skull and a burr-hole was drilled at the following coordinates: anteroposterior, -2.8 mm; mediolateral, $+1.6$ mm; dorsoventral, -5.5 mm. A custom-made cannula with a fused silica 1-mm stepped tip (Yin *et al.*, 2010) was used to deliver 15 μl of infusate unilaterally into the thalamus by convection-enhanced delivery (CED) at a rate of 0.5 μl/min. The total length of time for the infusion procedure was approximately 30 min plus a 2-min waiting period before cannula retraction to avoid reflux of infusate.

Each NHP was sedated with an intramuscular injection of a mixture of ketamine (Ketaset, 7 mg/kg) and xylazine (Rompun, 3 mg/kg). On sedation, each NHP was intubated

and placed on inhaled isoflurane (3%), and the head was positioned in a stereotactic frame. Two magnetic resonance imaging (MRI)-compatible cranial access ports (one per hemisphere) were secured to the skull with plastic screws (three per port) and, 2 weeks after port implantation, each NHP was sedated and transferred to the MRI facility. Cannula insertion and trajectory were established after acquiring high-resolution and T_2-weighted scans (described below). Briefly, a ceramic, fused silica (8 cm in length) reflux-resistant cannula with a 3-mm stepped tip (outer diameter, 0.5 μm; inner diameter, 200 μm), connected to the infusion line (infusate, AAV2-hASM/Gd or PBS–Gd), was lowered into the parenchyma, based on the best trajectory to the targeted region. Correct cannula placement within the target site was verified by visualization of vector (i.e., AAV2-hASM or PBS) coinfused with MRI-contrast tracer gadoteridol (Gd, 1 m*M*; ProHance) at the tip of the inserted cannula. The following infusion parameters were implemented: 1 μl/min (20 min), 1.5/2.0/2.5 μl/min (5 min each), and 3.0 μl/min (25 min for thalamic infusions and 50 min for brainstem infusions). Total infusion time per thalamus was 60 min and 85 min for brainstem. At the end of the procedure, each NHP received an intramuscular injection of buprenorphine (Buprenex, 0.01–0.05 mg/kg) and all animals were monitored for signs of discomfort by veterinary staff.

Magnetic resonance imaging

A 1.5-T Signa LX scanner (GE Medical Systems, Waukesha, WI) was used to acquire MR images starting with a high-resolution MP-RAGE (magnetization prepared-rapid acquisition gradient echo) scan and T_2-weighted images required for planning of cannula trajectory from the top of the array to the target site. After cannula insertion through the parenchymal tissue. T_1-weighted images were acquired with a spoiled GRASS (gradient-recalled acquisition in steady state) sequence and slice thickness of 1 mm, resulting in a 0.39-mm^3 voxel volume.

Neurological assessment and cage-side observations

In-life evaluation was conducted for all NHPs in this study. This included body weight and temperature measurements, cage-side observations (i.e., signs of paresis, locomotor/skin abnormalities), and neuroassessment (i.e., menace, gait, posture, nystagmus) performed by trained personnel blinded to the treatment groups (Supplementary Table S1; supplementary data are available online at www.liebertpub.com/hum).

Tissue processing

All animals were transcardially perfused with PBS and their brains were harvested. NHP brains were sliced coronally into two 3-mm blocks at the level of the thalamus. The rest of the brain was sliced into 6-mm blocks that were postfixed in 4% paraformaldehyde–PBS and cryoprotected in 30% sucrose. Of the two 3-mm blocks, the most anterior block sliced from the thalamus was collected and frozen rapidly in an isopropanol–dry ice bath for biochemical analysis; the other 3-mm block was embedded in paraffin and cut into 5-μm serial sections. Rat tissues, collected for biochemical analysis, were first dissected into specific regions (see illustration in Fig. 1a) and then frozen in dry ice-cooled isopentane (stored at −80°C or used immediately). All postfixed blocks were cut into 40-μm serial sections that were then processed further.

Immunoperoxidase staining

For hASM immunohistochemistry, a monoclonal antibody against hASM (biotinylated mouse anti-hASM, diluted 1:300; kindly supplied by Genzyme, Cambridge, MA) was used to detect the transgene. This antibody is not species specific and will detect endogenous enzyme. However, endogenous enzyme is so weakly expressed that vector-driven ASM expression is easily detectable, as we have previously shown (Salegio *et al.*, 2010). Briefly, sections were washed in PBS (3×5 min), quenched for endogenous peroxidase activity in PBS–1% H_2O_2 (30 min), and washed in PBS–1% Tween

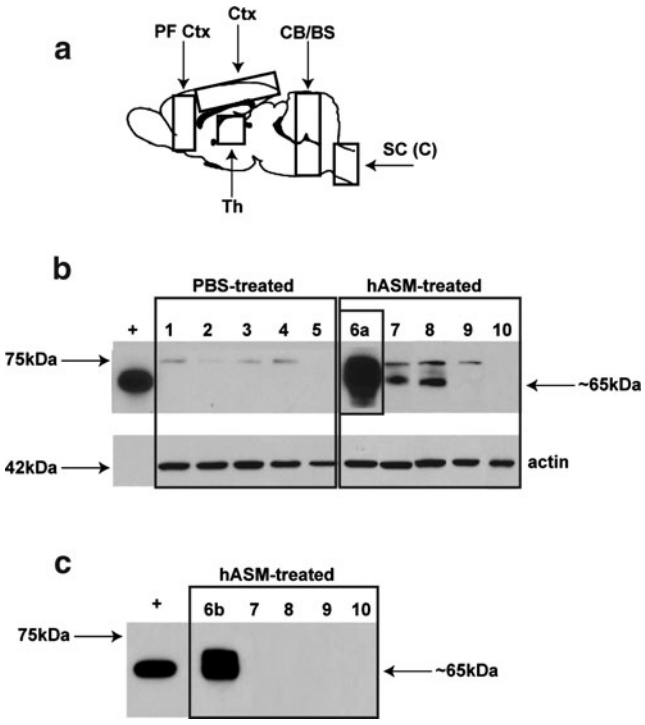

FIG. 1. Western blot analysis of tissue lysates from rats. **(a)** Schematic of the rat brain, indicating dissected regions used for Western blot analysis. CB/BS, cerebellum/brainstem; Ctx, cortex; PF Ctx, prefrontal cortex; SC (C), spinal cord cervical region; Th, thalamus. **(b)** Analysis of long-exposure Western blots indicated the presence of two proteins: (1) a 75-kDa band believed to represent endogenous acid sphingomyelinase (ASM), found in all samples except those collected from upper spinal cord regions, and (2) a 65-kDa band indicative of the mature enzyme and of similar molecular weight to the positive control (partially purified lysosomal hASM) and detected only in vector-treated samples from the thalamus, cortex, and prefrontal cortex. **(c)** In the shorter exposure Western blot, bands corresponding to the endogenous protein were not detected in any samples. Only samples collected from thalamic regions demonstrated the presence of a 65-kDa protein. Thalamus (lanes 1, 6a, and 6b), cortex (lanes 2 and 7), prefrontal cortex (lanes 3 and 8), cerebellum/brainstem (lanes 4 and 9), cervical/thoracic spinal cord (lanes 5 and 10), partially purified lysosomal hASM (+; positive control), and β-actin (loading control).

(PBST; 3×5 min). Sections were blocked for 30 min in Background Sniper (BS966 G; Biocare Medical, Concord, CA) and incubated overnight at 4°C with primary antibody (hASM) in DaVinci green diluent (PD900; Biocare Medical). The next day, after washing in PBST, sections were incubated with anti-biotin-M antibody (mouse, diluted 1:200, MB-9100; Vector Laboratories, Burlingame, CA) in Biocare DaVinci green diluent for 2 hr at ambient temperature. After incubation, sections were washed again (as described previously) and incubated in MACH 2 mouse HRP-polymer for 1 hr (MHRP520; Biocare Medical), washed in PBST, and developed with 3,3′-diaminobenzidine (DAB) for 2 min (DAB peroxidase substrate kit, SK-4100; Vector Laboratories). DAB-processed sections were washed in PBS, mounted on frosted slides, and counterstained with cresyl violet.

Immunostaining against inflammatory markers was used to detect the presence of microglia (rabbit-anti-Iba1, diluted 1:1000; Biocare Medical), T cells (mouse-anti-CD4, diluted 1:150; Biocare Medical), and macrophages (mouse-anti-CD68, diluted 1:1000; Dako, Carpinteria, CA), and were processed as per the hASM staining protocol described previously. The only exclusion was the anti-biotin-M step by directly incubating sections in either MACH 2 mouse or MACH 2 rabbit HRP-polymer (MHRP520; Biocare Medical), depending on the primary antibody used. DAB development time for Iba1 was 1.5 min, 3 min for CD68, and 2.5 min for CD4.

Immunofluorescence staining

Sections were costained with antibodies against hASM (diluted 1:50; Genzyme) and a chemokine involved in the attraction and activation of leukocytes (goat anti-human CCL5/RANTES; diluted 1:40; R&D Systems, Minneapolis, MN). Sections were washed in PBST (3×5 min), blocked in PBS–20% normal horse serum (Jackson ImmunoResearch, West Grove, PA) for 1 hr, and incubated with the primary antibodies in Biocare DaVinci green diluent (PD900; Biocare Medical) overnight at 4°C. After washing in PBST, sections were incubated with a cocktail of secondary antibodies against tetramethylrhodamine isothiocyanate (TRITC)-conjugated anti-mouse IgG (diluted 1:200; Jackson ImmunoResearch) and fluorescein isothiocyanate (FITC)-conjugated anti-goat IgG (diluted 1:200; Jackson ImmunoResearch) in PBST for 2 hr at room temperature, washed in PBS, and wet-mounted on frosted slides.

Histology: Hematoxylin and eosin

Slide-mounted sections were washed in graded alcohol (100, 95, and 70%; 3 min each), rehydrated in distilled water (twice; 5 min each), immersed in Surgipath hematoxylin (3 min; Leica Microsystems, Wetzlar, Germany) and washed in running tap water to remove any excess hematoxylin. After washing, sections were differentiated in 0.5% glacial acetic acid–70% alcohol (30 sec), washed in running tap water (2 min), immersed in bluing solution (30 sec), washed in running tap water, counterstained in Surgipath eosin (2 min; Leica Microsystems), and washed again. Last, sections were dehydrated in alcohol (95 and 100%; 3 min each), immersed in fresh xylene (twice; 3 min each), and preserved under coverslips.

In vitro *acid sphingomyelinase enzyme assay*

Tissues were homogenized in ice-cold buffer (20 m*M* Tris-HCl, pH 7.4, with added phosphatase inhibitor cocktails 1 and 2, and protease inhibitor cocktail (Sigma-Aldrich, St. Louis, MO) for 15–20 sec. Protein levels were determined with a bicinchoninic acid (BCA) protein determination kit (Pierce Biotechnology/Thermo Fisher Scientific, Rockford, IL) and normalized to 2 mg of protein per milliliter. Twenty-five micrograms of homogenate in a volume of 100 μl was added to 100 μl of reaction mixture to a final concentration of 100 μM porcine brain sphingomyelin (Avanti, Alabaster, AL), 1×10^5 cpm of [choline-*methyl*-^{14}C]sphingomyelin (specific radioactivity, 1.5×10^5 cpm/μl) kindly supplied by A. Bielawska (Medical University of South Carolina Lipidomics Core, Charleston, SC), presented in micelles containing 0.2% Triton X-100 in buffer (250 m*M* sodium acetate, 1 m*M* EDTA; pH 5.0). The reaction proceeded for 30 min at 37°C, and was terminated by the addition of 1.5 ml of chloroform–methanol (2:1, v/v) followed by 0.4 ml of Milli-Q water (modified Folch extraction). Samples were then vortexed briefly and subjected to centrifugation at 2000×*g* for 5 min at room temperature to separate phases. Aliquots (800 μl) of the upper (aqueous) phase were used for liquid scintillation counting. The assay was linear with respect to time and protein concentration, and substrate hydrolysis was less than 10%.

Western blotting

Tissues were homogenized as for the enzyme assay. Protein concentration was normalized and samples were boiled for 5 min after addition of 2× Laemmli buffer. Samples (25–50 μg) were subjected to sodium dodecyl sulfate–polyacrylamide gel electrophoresis (SDS–PAGE) (10% Tris-HCl) in the Criterion system (Bio-Rad, Hercules, CA) and transferred to nitrocellulose membranes. Membranes were blocked with 5% nonfat dried milk–PBST for 30–60 min and incubated overnight at 4°C with primary antibody (mouse anti-ASM-biotin, diluted 1:1000; Genzyme) and anti-β-actin (diluted 1:10,000; Sigma-Aldrich) in 5% milk–PBST. Membranes were washed with PBST (3×10 min) before incubation with horseradish peroxidase (HRP)-conjugated secondary antibody (goat anti-mouse, diluted 1:5000; anti-biotin–HRP, diluted 1:2500; Cell Signaling Technology, Danvers, MA) in 5% milk–PBST. After washing nitrocellulose in PBST (3×10 min), enhanced chemiluminescence was used to visualize bands. The development time between blots was adjusted for short (30 min) or long exposure (60 min). Note that SuperSignal substrate (Pierce Biotechnology/Thermo Fisher Scientific) was used to enhance the sensitivity of the longer exposure blot only. The positive control for hASM was partially purified human lysosomal hASM (kindly supplied by G. Smith, GlaxoSmithKline, Brentford, UK).

PCR detection of vector genomes

Total DNA was isolated from fresh-frozen rat samples with a Wizard genomic DNA purification kit (Promega, Madison, WI). Real-time qPCR was performed with primers specific for the CMV promoter sequence (forward primer, GCTCGTTTAGTGAACCGTCA; reverse primer, CCGGTGT CTTCTATGGAGGT), FAM-labeled detection probe (FAM-ATCGCCTGGAGACGCCATCCTCC-TAMRA), and TaqMan gene expression master mix (Applied Biosystems/Life Technologies, Foster City, CA). Rat tissue samples dissected from regions of the thalamus, prefrontal cortex, cerebral cortex,

cerebellum/brainstem, and spinal cord (cervical region) were run in triplicate with 5 μl of DNA sample per 25-μl reaction.

Sphingolipidomic analysis

Tissue was homogenized as described previously for enzyme activity and immunoblotting. Cellular homogenates (0.1–1.0 mg) were frozen at −80°C and then submitted for sphingolipidomic analysis by reversed-phase high-pressure liquid chromatography coupled with electrospray ionization followed by mass spectrometry. Analysis of sphingoid bases, ceramides, and sphingomyelins was performed on a Thermo Finnigan TSQ 7000 triple quadrupole mass spectrometer, operating in a multiple reaction-monitoring positive ionization mode, as described (Bielawski *et al.*, 2006).

Statistical analysis

Confidence intervals for comparisons of enzymatic activity in hASM-treated and controls, determined by Student *t* test, are expressed as *p* values for each comparison. All values represent means ± standard error of the mean.

Results

ASM bioactivity after thalamic infusion of AAV2-hASM in rats

We first determined the extent of ASM expression and activity of the enzyme over endogenous levels after infusion of AAV2-hASM into the thalamus of naive rats. Western blot analysis of tissues collected from rat thalamus, treated with either AAV2-hASM or PBS, demonstrated the presence of two proteins that reacted specifically with the ASM antibody. The minor band migrated at approximately 75 kDa and the more prominent at 65 kDa. The 75-kDa band likely represents pro-ASM, and the 65-kDa form mature L-SMase, which arises from C-terminal proteolytic processing. The 65-kDa band corresponds to partially purified lysosomal human ASM (positive control; Fig. 1b). The mature ASM protein was detected only in vector-treated samples, and was limited to regions of the thalamus, cortex, and prefrontal cortex. Note that the greatest amount of ASM protein was found at the site of primary infusion (i.e., thalamus) and this was not detected in any of the control samples. In shorter exposure immunoblots, the 65-kDa band was detectable only in samples collected from thalamic regions (Fig. 1c). To determine whether ASM in the cortex represented protein transported from thalamus or trafficking of vector through axonal connections, quantitative PCR of a fragment of the vector genome corresponding to a region of the CMV promoter was performed. Comparison of PCR results with ASM protein levels revealed that presence of ASM protein correlated closely with the presence of vector DNA, indicating that active viral transduction was required for induction of ASM protein (Table 1). Importantly, the lack of hASM immunoreactivity in brain regions where there was no evidence of viral transport (i.e., those regions without positive PCR for the CMV promoter) suggested that additional mechanisms posttranslational transport of ASM did not contribute significantly to the levels of ASM in other regions of the brain distant from the injection site.

To determine whether the expressed ASM was biologically active, the lysosomal activity of this enzyme, at a pH of 5.0, was calculated from the hydrolysis of [^{14}C]SM to [^{14}C]phosphorylcholine in the presence of EDTA, as previously described (Jenkins *et al.*, 2009). In rats (Table 1), AAV2-hASM infusion directed an 86% increase in ASM activity in thalamus (49.8 ± 7.0 vs. 26.8 ± 0.8 nmol/hr/mg protein in control tissue; $p < 0.03$). Slight increases in enzyme activity at lower confidence intervals were also found in other parts of the rat brain, such as the cortex (23%; treated, 38 ± 2.4; control, 30.9 ± 3.1; $p > 0.15$), prefrontal cortex (23%; treated, 37.2 ± 4.3; control, 30.3 ± 2.6; $p > 0.24$), cerebellum/brainstem (15%; treated, 39.4 ± 9.6; control, 34.3 ± 4.7; $p > 0.65$), and spinal cord (8%; treated, 14.8 ± 3.0; control, 13.7 ± 2.4; $p > 0.45$). This suggested that the enzyme was active and it correlated with the anterograde transport of this vector along thalamocortical projections (Kells *et al.*, 2009).

Table 1. Enzymatic Activity and Vector Genomes Within the Rat CNS

CNS region	Enzymatic activity (nmol/hr/mg protein)		Percentage of enzymatic activity above endogenous levels (fold)	Vector DNA (C_t)[a] Range
	Control (PBS)	Vector treated		
Th	26.8	49.8	86[b] (1.9-fold)	20.7–25.5
PF Ctx	30.9	38.0	23 (1.2-fold)	27.5–28.3
Ctx	30.3	37.2	23 (1.2-fold)	27.5–30.2
CB/BS	34.3	39.4	15 (1.1-fold)	33.3–37.9
SC (C)	13.7	14.8	8 (1.0-fold)	33.9–36.6

Th, thalamus; PF Ctx, prefrontal cortex; Ctx, cortex; CB/BS, cerebellum/brainstem; SC (C), spinal cord cervical region; Ct, cycle threshold.

[a]PCR results for control (non-vector-treated) samples were greater than 37 C_t.

[b]Significantly greater compared with endogenous levels ($p < 0.05$).

ASM bioactivity after AAV2-hASM infusion into NHP brain

Infusion into motor-sensitive regions of the CNS presents a greater risk of surgical complications compared with infusions into other brain regions. However, we have previously demonstrated that parenchymal CED in brainstem and thalamus was tolerated well by NHPs (Salegio *et al.*, 2010), and this can be partly attributed to precise control of infusion parameters via coinfusion of the therapeutic agent with the MRI tracer gadoteridol, thereby allowing real-time MRI monitoring and control of infusions. In this study we also found no significant differences in distribution between AAV2-hASM/Gd (high or low dose) and PBS–Gd in the brainstem or thalamus (data not shown). In agreement with our earlier studies (Salegio *et al.*, 2010), robust neuronal hASM expression was detected within regions directly targeted by the infusion in all of the vector-treated NHPs, regardless of survival time (Fig. 2). Western blot analysis of lysate samples collected from the thalamus of NHPs confirmed the presence of a 65-kDa band representative of the mature ASM protein in vector-treated samples (Table 2 and Supplementary Fig. S1), similar in size to a positive control derived from partially purified lysosomal human ASM (Jenkins *et al.*, 2010). Note that the 65-kDa band was more prominent in high-dose animals, suggesting greater

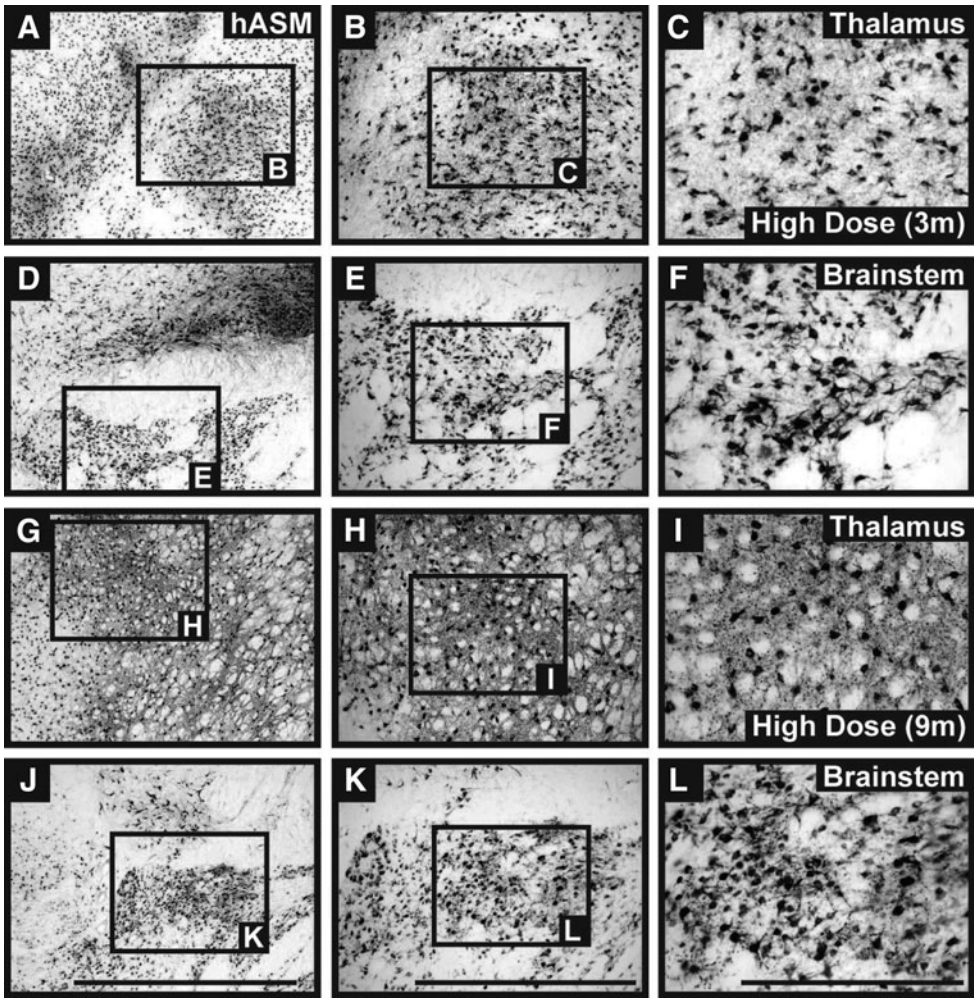

FIG. 2. Parenchymal neuronal ASM expression in nonhuman primates (NHPs). Immunostaining against hASM indicated strong neuronal transduction in both targeted regions (thalamus and brainstem). Expression of the hASM transgene was detected in all vector-treated brains irrespective of AAV dose and survival time point. No $hASM^+$ cells were found in the brains of control animals (data not shown). Scale bars: **(A, D, G,** and **J)** 2 mm; **(B, E, H,** and **K)** 1 mm; **(C, F, I,** and **L)** 500 μm.

production of the ASM protein with increasing doses of AAV2-hASM.

In NHPs, we found lysosomal ASM activity to be elevated in all vector-treated groups. Differences in ASM levels between animals in the same group are likely related to the variability in exact location of fresh tissue punches within the target region (Supplementary Fig. S2). Enzymatic activity of homogenized tissue collected from thalamic regions indicated increased ASM expression in excess of endogenous levels at high and low doses for short- and long-term survival animals (Table 2). Within the short-term survival group we found the increase in ASM activity to be 1.4-fold (NHP 3, LD) above detectable background levels, compared with a 7.4-fold increase in the high-dose animal (NHP 6). The greatest elevation in ASM activity, at 8.8-fold, was detected in one of the high-dose, long-term survival animals (NHP 8).

Table 2. Enzymatic Activity and Protein Detection Within the NHP Thalamus

NHP ID (dose, survival)	*Enzymatic activity (nmol/hr/mg protein)*	*Percentage of enzymatic activity above endogenous levels (fold)*
Controls (3m)[a]	47.7	n/a
NHP 3 (LD, 3m)	64.6	35 (1.4-fold)
NHP 5 (HD, 3m)	144	202 (3.0-fold)
NHP 6 (HD, 3m)	351	636 (7.4-fold)
NHP 7 (LD, 9m)	340	612 (7.1-fold)
NHP 8 (HD, 9m)	418	776 (8.8-fold)

3m, 3 months; 9m, 9 months; L/HD, low/high dose; +/−, band present/absent in Western blot; n/a, not applicable.

[a]Enzymatic activity for controls (3m) is represented by the mean from two PBS-control animals (NHPs 1 and 2). Note that NHP 4 was not included in this analysis as the 6-mm punch was taken outside the area of ASM expression, and thus no enzyme activity was detected (see Supplementary Fig. S2).

Behavioral deficits in NHPs treated with AAV2-hASM

To closely monitor for the development of any adverse effects related to AAV2-hASM infusion, trained animal staff blinded to the experimental groups performed in-life observations including cage side (once daily for five consecutive days), weight monitoring (once every 2 weeks), and blood analysis (before and after treatment administration) throughout the course of the study. Surprisingly, we found that all of the vector-treated NHPs experienced some type of abnormality manifested in the form of neurological deterioration, weight loss, and/or abnormal blood results (Supplementary Table S1). Some of the most severe side effects included hemiparesis in both hind limbs and consequently

led to early necropsy of one of the high-dose animals. No abnormal changes were observed in any of the PBS-treated animals, suggesting that these side effects present in the AAV2-hASM-treated animals were not caused by the surgery and/or infusion procedure.

Elevations in proinflammatory sphingolipids after AAV2-ASM infusion

Given the significant behavioral and neurophysiological alterations evident in the treated NHPs, and not in the saline control NHPs, we reasoned that the action of ASM was itself responsible for these effects. Sphingolipidomic analysis of thalami from control and AAV2-hASM-treated NHPs was performed to evaluate the impact of ASM on the sphingolipid profile. Lipid analysis revealed that increased hASM expression resulted in reduced levels of sphingomyelin (the primary substrate of ASM), as would be expected. Interestingly, with increasing hASM expression, ceramide (the product of sphingomyelin hydrolysis) levels were not elevated, but rather were slightly decreased compared with control samples (Fig. 3A and B). Elevation in downstream metabolites of ceramide—sphingosine and sphingosine 1-phosphate—in response to hASM was observed only in the high-dose treatment group at the 3-month time point (Fig. 3C and D). These data demonstrate that hASM toxicity may be associated with sphingosine and/or sphingosine 1-phosphate accumulation at higher doses of hASM, rather than alterations in SM and ceramide levels.

Toxicity and chemokine upregulation induced by hASM overexpression

Bioactive sphingolipids such as sphingosine and sphingosine 1-phosphate (S1P) have been implicated in diverse pathophysiological processes including ischemia–reperfusion injury, elaboration of chemokines, chemotaxis, wound healing, and cell death (Theilmeier *et al.*, 2006). To determine whether alterations in levels of these bioactive sphingolipids correlated with alterations in tissue architecture or composition, we first performed hematoxylin and eosin (H&E) staining of NHP brain slices. H&E staining revealed abnormal tissue pathology in AAV2-hASM-treated animals (Fig. 4A and B), that was not seen in control brains, and included signs of gliosis and cellular infiltrates. Immunohistochemistry indicated an increased presence of inflammatory cells in brain regions proximal to the site of AAV2-hASM infusion, specifically activated macrophages ($CD68^+$), microglia ($Iba1^+$), T cells ($CD4^+$; Fig. 4C–H), and antigen-presenting cells ($MHC\text{-}II^+$; data not shown). Note that brains from control animals demonstrated only the normal, mild gliotic response to cannula penetration into the parenchyma (Fig. 4I–P). In addition, histopathological analysis of these brains revealed a significant inflammatory response evident by the formation of perivascular cuffs in vector-treated animals as compared with controls (Fig. 5). Given that in the past ASM has been suggested to promote cell death, we performed TUNEL (terminal deoxynucleotidyltransferase dUTP nick end labeling) staining. However, no evidence of cell death was found within regions of hASM expression and/or inflammatory response (data not shown). Therefore, the induction of ASM resulted in a marked cellular inflammatory response but no overt tissue damage. In addition, no signs of toxicity were found in vector- or PBS-treated rats (data not shown), suggesting species-specific toxicity against hASM transgene.

Next, we investigated the possible molecular basis for this ASM-driven inflammatory response. Although sphingolipids have been shown to modulate inflammation in a variety of ways, CCL5/RANTES has been identified as a novel mediator of ASM-driven sphingolipid signaling, based on screening for cytokine/chemokine effectors of ASM. Importantly, ASM was

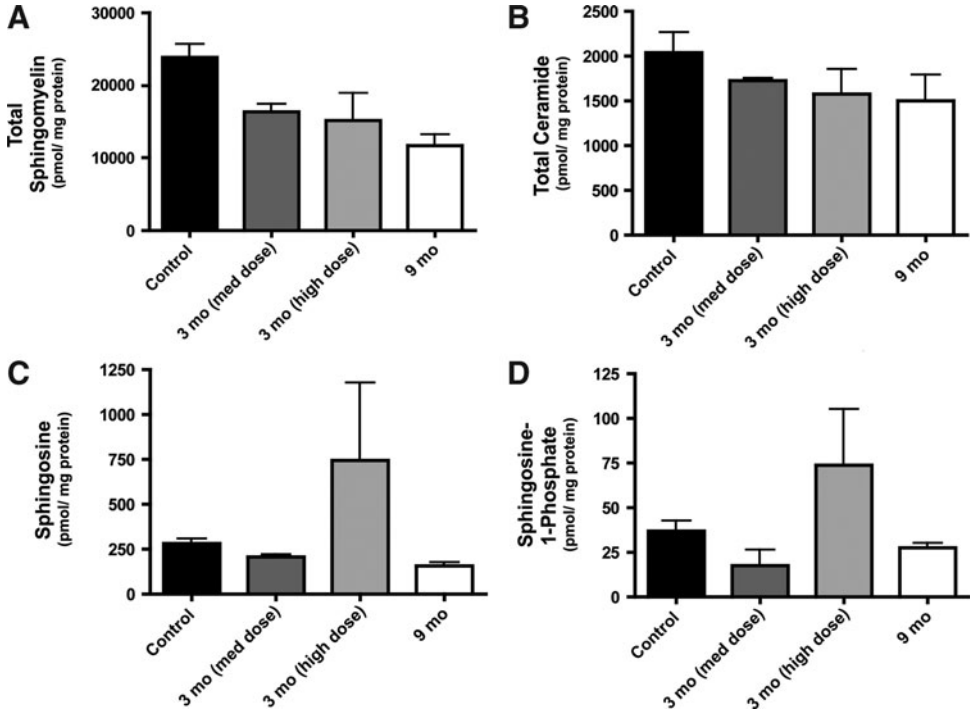

FIG. 3. Lipid analysis of NHP brain samples. Thalamic homogenates from PBS-treated controls and AAV2-hASM-treated NHPs were submitted for sphingolipidomic analysis, as described in Materials and Methods. Data are expressed as picomoles per milligram of total protein for each lipid or group of lipids analyzed ($n=2$ per group). **(A)** Total sphingomyelin; **(B)** total ceramide; **(C)** sphingosine; **(D)** sphingosine 1-phosphate.

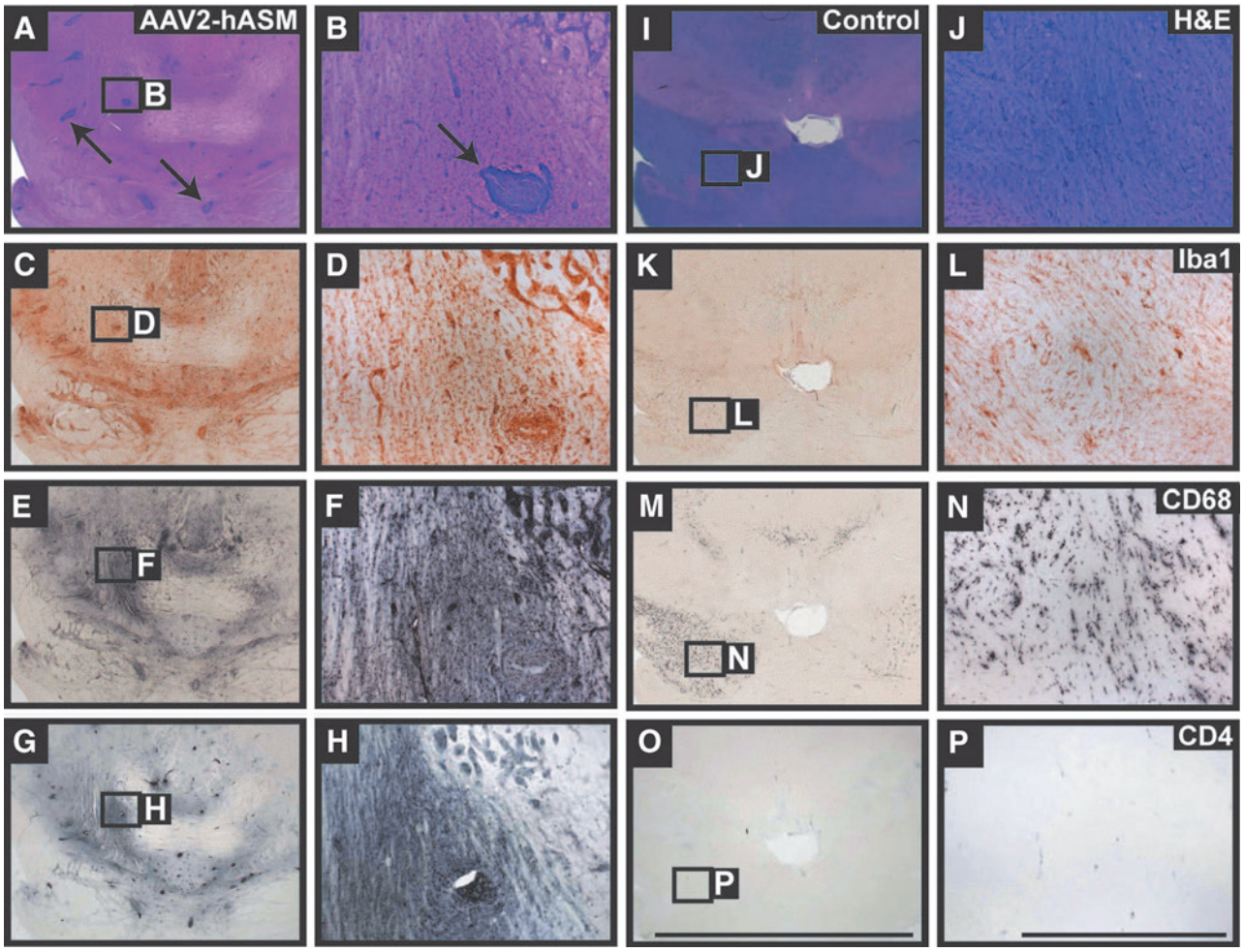

FIG. 4. Brain pathology and inflammatory cell recruitment. Histological examination of vector-treated NHP brains demonstrated significant pathological signs (**A** and **B,** arrows) not observed in PBS-treated controls. Immunostaining of thalamic and brainstem regions in hASM-infused animals indicated robust infiltration and activation of inflammatory cells consisting mainly of microglia (**C** and **D,** $Iba1^+$), macrophages (**E** and **F,** $CD68^+$), and activated T cells (**G** and **H,** $CD4^+$). Expression of inflammatory cells in control animals represents the normal immune response to cannula penetration and the convection-enhanced delivery (CED) procedure within the parenchyma **(I–P)**. Scale bars: Low-magnification panels, 10 mm; high-magnification panels, 1 mm. Color images available online at www.liebertpub.com/hum

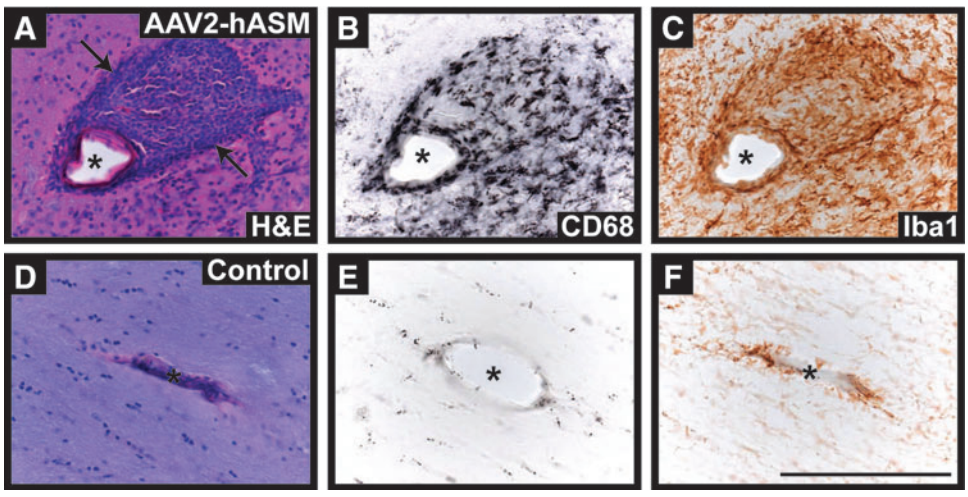

FIG. 5. Perivascular cuffing in AAV2-hASM-treated NHP brains. **(A)** Hematoxylin and eosin-processed sections from vector-treated animals (high dose, 3-month survival) indicate the presence of cuffing (arrows) around blood vessels (asterisks); cuffs were composed of macrophage ($CD68^+$) and microglial ($Iba1^+$) infiltrates **(B** and **C)**, as compared with PBS-treated control tissue **(D–F)**. Scale bar: 200 μm. Color images available online at www.liebertpub.com/hum

shown to be both necessary and sufficient to promote upregulation of CCL5 (Jenkins *et al.*, 2011), and CCL5 was the primary chemokine from a panel of more than 30 chemokines that was regulated by ASM. To determine whether CCL5 levels were increased as a result of hASM transgene expression, we performed immunofluorescence staining for hASM and CCL5 in both control and vector-treated NHPs. Indeed, immunofluorescence studies showed that neuronal ASM overexpression was associated with pronounced upregulation of CCL5, a potent chemokine associated with leukocyte recruitment (Fig. 6). Furthermore, analysis of CCL5 levels in brain homogenates by ELISA revealed similar upregulation of CCL5, although levels were most elevated in the high-dose group at the 3-month time point (Supplementary Fig. S3). These results demonstrate that ASM induces CCL5 expression *in vivo*, in agreement with previous *in vitro* data (Jenkins *et al.*, 2011).

Discussion

The purpose of this study was to investigate the long-term consequences of overexpression of hASM in neurons in the naive NHP brain as part of a larger effort to evaluate the safety and efficacy of virus-mediated delivery of hASM. To assure ourselves of the bioactivity of the AAV vector, we first assessed safety and efficacy in the rat. Western blotting for ASM in rat brain demonstrated abundant ASM expression and enhanced active enzyme in tissue extracts. Thalamic expression of ASM appeared to be much greater in NHPs than in rats, even though the rats received about 4-fold more

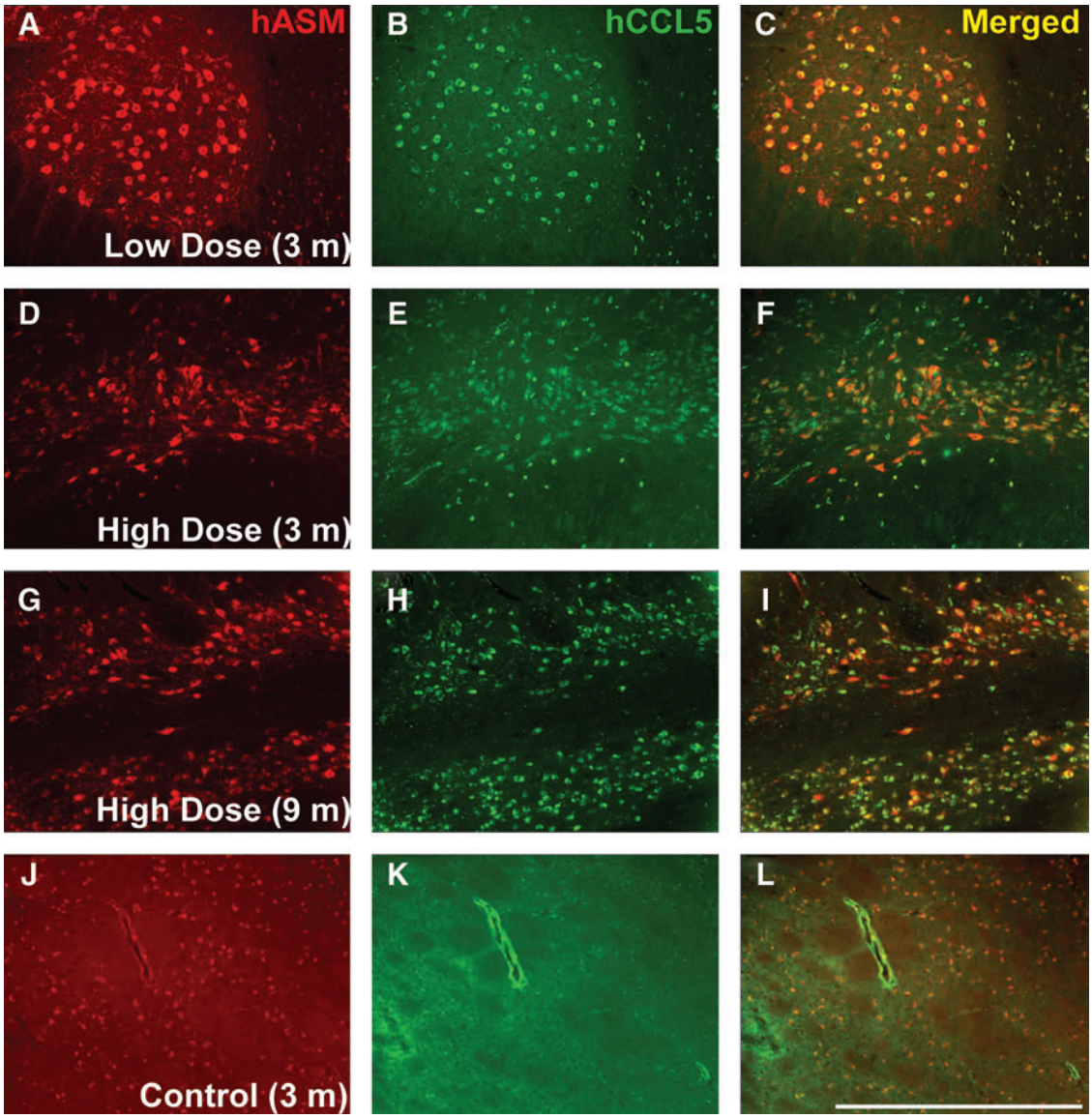

FIG. 6. Neuronal coexpression of hASM and CCL5. Immunofluorescence staining for hASM (red) and the chemokine CCL5/RANTES (green) revealed neuronal coexpression of hASM and CCL5 in vector-treated animals independent of AAV dose and survival (**A–I,** yellow), compared with PBS-treated controls **(J–L)**. Note that neurons staining for both hASM and CCL5 were found only within the brains of NHPs infused with AAV2-hASM. Scale bar: **(A–L)** 1 mm. Color images available online at www.liebertpub.com/hum

vector per unit volume of target tissue than did NHPs. This may be due to species differences in protein stability and better interaction of human ASM with partner proteins in NHPs than in rodents. However, further investigation will be required to determine whether this is so.

A separate conclusion from this study is that hASM expression appears to be limited by viral distribution. Previously, we have shown that AAV2 undergoes significant anterograde axonal transport from thalamus to cortex (Kells *et al.*, 2009). In the present study, we confirm that the same phenomenon occurs in rats as well as NHPs, and this technique allowed us to explore the relationship between transport of AAV2-hASM genomes and transport of ASM itself. Although there is evidence of anterograde transport of AAV2 from thalamus to cortex (Fig. 1 and Table 1), we found no evidence of transport of enzyme to more distal regions of the rat brain. Cortical regions that expressed hASM were also positive by quantitative PCR of vector. This also seems to be true in the present long-term NHP experiments. This is concerning because partial secretion of ASM and uptake by neighboring cells has been previously documented to occur (Schissel *et al.*, 1998). However, the efficiency of this process seems to be quite low in normal macrophages and even worse in macrophages from NPD knockout mice (Dhami and Schuchman, 2004). Because expectations of efficacy in gene therapy for LSDs in general, and NPD in particular, rest on the thesis that enzyme is secreted and subsequent taken up by neighboring cells, we expected to see significant augmentation of ASM activity in regions of brain distal to those domains demonstrated to contain vector DNA. It might be argued that, because the antibody we used was not able to distinguish between transgene and endogenous enzyme, we might have failed to detect transport. We believe this is not the case, because the present study is in agreement with our previous study demonstrating a strong correlation between tagged and untagged ASM expression (Salegio *et al.*, 2010). If there were significant intercellular transport of ASM, we believe that it would have been detectable by immunohistochemistry, Western blotting, or enzyme activity. That is not to say, however, that secretion of hASM does not occur at all, because it has been amply shown in transfected cells (He *et al.*, 1999). However, it is unclear how efficient this process really is *in vivo*. In an efficacy study in $ASM^{-/-}$ mice, Passini and colleagues demonstrated a remarkable correlation between *in situ* ASM mRNA hybridization and ASM immunohistochemistry (Passini *et al.*, 2005) after stereotactic injection of AAV2-hASM into hippocampus. In addition, we evaluated zinc-dependent secretory ASM (S-SMase) activity in the cerebrospinal fluid from treated and untreated NHPs as a measure of the extent of extracellular secretion of hASM after viral transduction. We found only a modest elevation in S-SMase activity in one of two NHPs treated for 9 months with high-dose AAV2-hASM (data not shown). This, together with our studies in rats and NHPs, suggests that the efficiency of this process is insufficient to be a significant factor in gene therapy for NPD. It is possible that this lack of transport is a specific feature of neuronal expression, although future studies on the transcellular transport of ASM will be required to better characterize this process.

Notably, the ASM gene gives rise to two distinct proteins—lysosomal sphingomyelinase (L-SMase) and secretory sphingomyelinase (S-SMase)—through differential trafficking of a shared pro-ASM precursor (Jenkins *et al.*, 2009). Studies have begun to define distinct physiological functions for L-SMase and S-SMase, with S-SMase emerging as a mediator of the inflammatory response (Jenkins *et al.*, 2011) and L-SMase serving as the primary enzyme responsible for the metabolism of lysosomal SM. L-SMase is likely the primary enzyme responsible for metabolism of lysosomal SM, and its formation begins with the targeting of the pro-ASM precursor to the endolysosomal compartment through the mannose 6-phosphate receptor and sortillin pathways. Subsequently, pro-ASM undergoes proteolytic processing and tightly coordinates with zinc to form the mature L-SMase (Schissel *et al.*, 1998). Data have demonstrated that C-terminal proteolytic processing of pro-ASM is an essential step for L-SMase formation, established mature L-SMase as a 65-kDa protein, and suggested that processing of pro-ASM is the rate-limiting step in L-SMase formation (Jenkins *et al.*, 2011).

More concerning than the apparent lack of intercellular ASM transport in NHPs was the pronounced behavioral toxicity triggered by AAV2-hASM delivery into NHP brain. In all high-dose animals, but not in controls, abnormal gait and posture were readily apparent, and two high-dose animals suffered hind-limb paresis and weight loss. One low-dose animal suffered such severe weight loss that it had to be killed earlier than planned, although it is unclear whether this was solely an effect of treatment. Other than that one outlier, locomotion and gait were not abnormal in the low-dose group but severe and pervasive in the high-dose group. These data suggest that the high dose of AAV2-hASM delivered exceeded a maximal tolerated dose, and indicate further that the low dose is close to, but still exceeds, a "no adverse event" level (NOAEL). Clearly, further experiments are required to understand the dose dependence of toxicity more comprehensively, especially in animals such as NHPs, which are more similar to human subjects and appear to be sensitive to hASM overexpression whereas rodents appear more resistant.

A potential issue with ASM replacement therapy is the possibility of generating excess products of sphingomyelin breakdown. Ceramide, a direct product of ASM-mediated digestion of SM, is an intracellular signaling molecule that can trigger both cell survival and cell death (Zeidan and Hannun, 2010). However, ceramide levels were lower in vector-treated NHPs than in controls. In contrast, downstream metabolites of ceramide—sphingosine and S1P—were both elevated. In addition, we observed brisk upregulation of the chemokine CCL5 (formerly known as RANTES), a potent chemokine known to promote trafficking of leukocytes (Levy, 2009). This phenomenon was seen in NHPs, regardless of vector dose, although quantitative data from CCL5 ELISA indicated the highest levels were present in the short-term (3-month) high-dose group. Accordingly, perivascular cuffing was seen in treated NHPs but not in control animals. These data correlate well with *in vitro* experiments that indicate a direct effect of hASM on CCL5 upregulation (Jenkins *et al.*, 2011). These studies showed that CCL5 upregulation depends on the presence of ASM in the constitutive secretion pathway. Overexpression in MCF7 breast cancer cells of mutant ASM that is directed solely to lysosomes did not upregulate CCL5, suggesting that non-lysosomal ASM was responsible for induction of CCL5. Importantly, acid ceramidase (AC) was also shown to be

requisite for the upregulation of CCL5, and simultaneous overexpression of ASM and AC resulted in synergistic elevations in CCL5, consistent with a role for sphingosine. Furthermore, CCL5 levels were significantly elevated in cells lacking sphingosine kinases, suggesting that the formation of S1P from sphingosine was at the least dispensable for induction of CCL5. Further experiments are needed, however, to establish whether this is indeed the correct explanation for this inflammatory effect of ASM overexpression. It should be noted that CCL5 upregulation and leukocyte accumulation do not seem to be the sole cause of locomotor effects after AAV2-hASM administration, because CCL5 was also detected in low-dose animals where less behavioral deficit was observed. However, the highest levels of sphingosine/S1P and CCL5 were present in the short-term (3-month) high-dose group, both members of which exhibited profound neurological and systemic symptoms, indicating that there may be a threshold at which the local CNS inflammation becomes overwhelming. That CCL5 levels were returning to normal at 9 months may also indicate that CCL5 is a more proximal event, and that the inflammatory cascade is more advanced at this time point. Rigorous temporal analysis of the expression of inflammatory mediators in brain parenchyma is obviously not practical or feasible in this model, but would be expected to reveal a sequential upregulation of ASM, sphingosine/S1P, CCL5, and then gliosis and inflammation (Skuljec *et al.*, 2011). From the perspective of ASM-mediated inflammatory signaling, this unexpected result is not only the first report of a direct role for ASM-driven CCL5 upregulation *in vivo*, but also provides evidence to support a role for ASM in upregulating CCL5 elaboration that in turn indicates that ASM-driven CCL5 upregulation is biologically relevant (i.e., is associated with gliosis and inflammation). These results further indicate that, even at high levels of expression, ASM does not induce cell death *in vivo*, and suggests perhaps that mutants of ASM that lack the capacity to promote CCL5 upregulation (Jenkins *et al.*, 2010) may be particularly attractive for the development of novel therapeutic approaches for NPD, because they may be effective at reducing lysosomal SM storage without promoting inflammation when exceeding therapeutic levels.

This study has profound implications for the development of a gene therapy for NPD-A. First, we found no evidence for significant transport of ASM from transfected neurons to other cells, even those in close proximity to the transduced neurons. If this holds even with vectors that transduce nonneuronal cells, such as AAV9 (Foust *et al.*, 2009; Gray *et al.*, 2011), the difficulty of transducing sufficient numbers of cells in the brain of patients with NPDA to effect therapeutic benefit may prove too daunting a task. However, if one considers the experience of enzyme replacement for other LSDs, such as Gaucher disease, then engineering of the native enzyme to enhance intercellular transport and uptake may be required (Zhang *et al.*, 2011). On the other hand, this study demonstrated that AAV2-hASM at a relatively low dose caused only slight behavioral defects if any. Whether these doses are physiologically effective remains to be seen. However, we have now defined in a primate some dose-related toxicities that should serve us well in the next iteration of the development of a gene therapy for this rare but lethal disease.

Acknowledgments

This work was supported by the National Institute of Neurological Disorders and Stroke, National Institutes of Health (grant R01-NS056107-01) to K.S.B. and by the National Institutes of Health (grant P01-CA097132) to Y.A.H. The authors thank Dr. Stephen DeArmond for human brain tissue, Dr. Alicja Bielawska for radioactive sphingomyelin, and Genzyme for anti-ASM antibody. The authors are grateful also to Dr. Gary Smith (GlaxoSmithKline) for the generous gift of partially purified human lysosomal ASM.

Author Disclosure Statement

No competing financial interests exist.

References

Amalfitano, A., McVie-Wylie, A.J., Hu, H., *et al.* (1999). Systemic correction of the muscle disorder glycogen storage disease type II after hepatic targeting of a modified adenovirus vector encoding human acid-α-glucosidase. Proc. Natl. Acad. Sci. U.S.A. 96, 8861–8866.

Ayuso, E., Mingozzi, F., Montane, J., *et al.* (2010). High AAV vector purity results in serotype- and tissue-independent enhancement of transduction efficiency. Gene Ther. 17, 503–510.

Barranger, J.M., and Novelli, E.A. (2001). Gene therapy for lysosomal storage disorders. Expert Opin. Biol. Ther. 1, 857–867.

Bielawski, J., Szulc, Z.M., Hannun, Y.A., *et al.* (2006). Simultaneous quantitative analysis of bioactive sphingolipids by high-performance liquid chromatography-tandem mass spectrometry. Methods 39, 82–91.

Bosch, A., Perret, E., Desmaris, N., *et al.* (2000). Reversal of pathology in the entire brain of mucopolysaccharidosis type VII mice after lentivirus-mediated gene transfer. Hum. Gene Ther. 11, 1139–1150.

Cearley, C.N., and Wolfe, J.H. (2007). A single injection of an adeno-associated virus vector into nuclei with divergent connections results in widespread vector distribution in the brain and global correction of a neurogenetic disease. J. Neurosci. 27, 9928–9940.

Dhami, R., and Schuchman, E.H. (2004). Mannose 6-phosphate receptor-mediated uptake is defective in acid sphingomyelinase-deficient macrophages: Implications for Niemann-Pick disease enzyme replacement therapy. J. Biol. Chem. 279, 1526–1532.

Dodge, J.C., Clarke, J., Song, A., *et al.* (2005). Gene transfer of human acid sphingomyelinase corrects neuropathology and motor deficits in a mouse model of Niemann-Pick type A disease. Proc. Natl. Acad. Sci. U.S.A. 102, 17822–17827.

Foust, K.D., Nurre, E., Montgomery, C.L., *et al.* (2009). Intravascular AAV9 preferentially targets neonatal neurons and adult astrocytes. Nat. Biotechnol. 27, 59–65.

Graber, D., Salvayre, R., and Levade, T. (1994). Accurate differentiation of neuronopathic and nonneuronopathic forms of Niemann-Pick disease by evaluation of the effective residual lysosomal sphingomyelinase activity in intact cells. J. Neurochem. 63, 1060–1068.

Gray, S.J., Matagne, V., Bachaboina, L., *et al.* (2011). Preclinical differences of intravascular AAV9 delivery to neurons and glia: A comparative study of adult mice and nonhuman primates. Mol. Ther. 19, 1058–1069.

He, X., Miranda, S.R., Xiong, X., *et al.* (1999). Characterization of human acid sphingomyelinase purified from the media of overexpressing Chinese hamster ovary cells. Biochim. Biophys. Acta 1432, 251–264.

Hsich, G., Sena-Esteves, M., and Breakefield, X.O. (2002). Critical issues in gene therapy for neurologic disease. Hum. Gene Ther. 13, 579–604.

Jenkins, R.W., Canals, D., and Hannun, Y.A. (2009). Roles and regulation of secretory and lysosomal acid sphingomyelinase. Cell Signal. 21, 836–846.

Jenkins, R.W., Canals, D., Idkowiak-Baldys, J., *et al.* (2010). Regulated secretion of acid sphingomyelinase: Implications for selectivity of ceramide formation. J. Biol. Chem. 285, 35706–35718.

Jenkins, R.W., Clarke, C.J., Canals, D., *et al.* (2011). Regulation of CC ligand 5/RANTES by acid sphingomyelinase and acid ceramidase. J. Biol. Chem. 286, 13292–13303.

Kells, A.P., Hadaczek, P., Yin, D., *et al.* (2009). Efficient gene therapy-based method for the delivery of therapeutics to primate cortex. Proc. Natl. Acad. Sci. U.S.A. 106, 2407–2411.

Kim, E.Y., Hong, Y.B., Lai, Z., *et al.* (2004). Expression and secretion of human glucocerebrosidase mediated by recombinant lentivirus vectors *in vitro* and *in vivo*: Implications for gene therapy of Gaucher disease. Biochem. Biophys. Res. Commun. 318, 381–390.

Kitagawa T. (1987). An animal model of human acid sphingomyelinase deficiency (Niemann-Pick disease) and the study of its enzyme replacement (the Japan Society of Human Genetics award lecture). Jinrui Idengaku Zasshi 32, 55–69.

Levy, J.A. (2009). The unexpected pleiotropic activities of RANTES. J. Immunol. 182, 3945–3946.

Matsushita, T., Elliger, S., Elliger, C., *et al.* (1998). Adeno-associated virus vectors can be efficiently produced without helper virus. Gene Ther. 5, 938–945.

Miranda, S.R., He, X., Simonaro, C.M., *et al.* (2000). Infusion of recombinant human acid sphingomyelinase into Niemann-Pick disease mice leads to visceral, but not neurological, correction of the pathophysiology. FASEB J. 14, 1988–1995.

Otterbach, B., and Stoffel, W. (1995). Acid sphingomyelinase-deficient mice mimic the neurovisceral form of human lysosomal storage disease (Niemann-Pick disease). Cell 81, 1053–1061.

Passini, M.A., Macauley, S.L., Huff, M.R., *et al.* (2005). AAV vector-mediated correction of brain pathology in a mouse model of Niemann-Pick A disease. Mol. Ther. 11, 754–762.

Passini, M.A., Bu, J., Fidler, J.A., *et al.* (2007). Combination brain and systemic injections of AAV provide maximal functional and survival benefits in the Niemann-Pick mouse. Proc. Natl. Acad. Sci. U.S.A. 104, 9505–9510.

Peltola, M., Kyttala, A., Heinonen, O., *et al.* (1998). Adenovirus-mediated gene transfer results in decreased lysosomal storage in brain and total correction in liver of aspartylglucosaminuria (AGU) mouse. Gene Ther. 5, 1314–1321.

Salegio, E.A., Kells, A.P., Richardson, R.M., *et al.* (2010). Magnetic resonance imaging-guided delivery of adeno-associated virus type 2 to the primate brain for the treatment of lysosomal storage disorders. Hum. Gene Ther. 21, 1093–1103.

Schissel, S.L., Keesler, G.A., Schuchman, E.H., *et al.* (1998). The cellular trafficking and zinc dependence of secretory and lysosomal sphingomyelinase, two products of the acid sphingomyelinase gene. J. Biol. Chem. 273, 18250–18259.

Skuljec, J., Sun, H., Pul, R., *et al.* (2011). CCL5 induces a pro-inflammatory profile in microglia *in vitro*. Cell Immunol. 270, 164–171.

Theilmeier, G., Schmidt, C., Herrmann, J., *et al.* (2006). High-density lipoproteins and their constituent, sphingosine-1-phosphate, directly protect the heart against ischemia/reperfusion injury *in vivo* via the S1P3 lysophospholipid receptor. Circulation 114, 1403–1409.

Watson, D.J., and Wolfe, J.H. (2003). Lentiviral vectors for gene transfer to the central nervous system: Applications in lysosomal storage disease animal models. Methods Mol. Med. 76, 383–403.

Yin, D., Forsayeth, J., and Bankiewicz, K.S. (2010). Optimized cannula design and placement for convection-enhanced delivery in rat striatum. J. Neurosci. Methods 187, 46–51.

Zeidan, Y.H., and Hannun, Y.A. (2010). The acid sphingomyelinase/ceramide pathway: Biomedical significance and mechanisms of regulation. Curr. Mol. Med. 10, 454–466.

Zhang, X.S., Brondyk, W., Lydon, J.T., *et al.* (2011). Biotherapeutic target or sink: Analysis of the macrophage mannose receptor tissue distribution in murine models of lysosomal storage diseases. J. Inherit. Metab. Dis 34, 795–809.

Zhou, H., Linke, R.P., Schaefer, H.E., *et al.* (1995). Progressive liver failure in a patient with adult Niemann-Pick disease associated with generalized AL amyloidosis. Virchows Arch. 426, 635–639.

Ziegler, R.J., Yew, N.S., Li, C., *et al.* (1999). Correction of enzymatic and lysosomal storage defects in Fabry mice by adenovirus-mediated gene transfer. Hum. Gene Ther. 10, 1667–1682.

Address correspondence to:
Dr. John Forsayeth
Department of Neurological Surgery
University of California San Francisco
1855 Folsom Street, MCB, Room 226
San Francisco, CA 94103-0555

E-mail: john.forsayeth@ucsf.edu

Received for publication March 5, 2012;
accepted after revision April 29, 2012.

Published online: May 10, 2012.